Characterization of the $TiSiO_4$ structure and its pressure-induced phase transformations: Density functional theory study

L. Gracia,[1] A. Beltrán,[1] and D. Errandonea[2]
[1]*MALTA Consolider Team, Departament de Química Física I Analítica, Universitat Jaume I, Campus de Riu Sec, Castelló E-12080, Spain*
[2]*MALTA Consolider Team, Departament de Física Aplicada–ICMUV, Fundació General de la Universitat de València, Burjassot, 46100 Valencia, Spain*

(Received 13 May 2009; revised manuscript received 24 June 2009; published 15 September 2009)

Theoretical investigations concerning the possible titanium silicate polymorphs have been performed using density functional theory at B3LYP level. Total-energy calculations and geometry optimizations have been carried out for all phases involved. The following sequence of pressure-driven structural transitions has been found: $CrVO_4$-type, *Cmcm* (in parenthesis the transition pressure), → zircon-type, $I4_1/amd$ (0.8 GPa), → scheelite-type, $I4_1/a$ (3.8 GPa). At higher pressure the last phase is found to be stable at least up to 25 GPa. The equation of state of the different polymorphs is also reported. We found that the highest bulk modulus corresponds to the zircon and scheelite phases with values of 248 and 238 GPa, respectively. The orthorhombic *Cmcm* phase is the most compressible of all the studied structures with a bulk modulus of 124 GPa, being also the most stable phase at ambient pressure. Finally, calculations of the electronic structure, vibrational and dielectric properties of $TiSiO_4$ are also reported.

DOI: 10.1103/PhysRevB.80.094105 PACS number(s): 64.60.−i, 62.50.−p, 61.50.Ks, 63.20.D−

I. INTRODUCTION

The ternary system consisting of mixtures of TiO_2 and SiO_2 is important for applications in a wide variety of domains. Dispersed TiO_2 in a SiO_2 matrix has shown very interesting properties for its use as a catalyst and a catalytic support material.[1] In addition, by mixing TiO_2 and SiO_2, it is possible to vary the refractive index of the composite material from that of SiO_2 (1.45) to that of TiO_2 (2.55).[2,3] This precise control of the refractive index over such a wide range has been used for the fabrication of several optical devices such as passive or active waveguides, antireflective coatings, and notch filters.[4–6] On the other hand, titanium silicate or TiO_2/SiO_2 mixed-oxide thin films offers the possibility to reach extremely high dielectric-constant values.[7–10] This fact is fundamental for achieving one of the semiconductor industry goals, the scaling of metal-oxide-semiconductor field-effect transistors (MOSFET) to smaller and smaller physical dimensions.

Transition metal orthosilicates, such as $ZrSiO_4$ (zircon) and $HfSiO_4$ (hafnon), are well known minerals, which can be also artificially produced. At ambient conditions, they crystallize in the tetragonal zircon structure [space group (SG): $I4_1/amd$, $Z=4$].[11] Natural zircon is a common mineral in Earth's crust, and its ability to resist physical and chemical alteration places it among the most commonly used minerals to date geological events.[12] It has been also suggested that materials, such as zircon, could effectively retain radioactive waste.[13,14] Because of the above described reasons, this family of silicates is subject of a wide range of studies in earth sciences, radioactive waste related research, and materials science. In particular, several high-pressure studies have been performed in $ZrSiO_4$ (Refs. 15–17) and $HfSiO_4$.[18] However; much less efforts have been dedicated to the study of $TiSiO_4$.

By analogy with $ZrSiO_4$ and $HfSiO_4$, the structural, vibrational, and dielectric properties of $TiSiO_4$, at ambient pressure, have been theoretically studied assuming a zircon-type structure.[19] However, $TiSiO_4$ has been up to now obtained only as an amorphous thin film.[20] On the other hand, based upon crystal-chemistry arguments,[21] in addition to the zircon-type structure, other structures like the tetragonal scheelite structure (SG: $I4_1/a$, $Z=4$) (Ref. 22) and the orthorhombic $CrVO_4$-type structure (SG: *Cmcm*, $Z=4$) (Ref. 23) have been proposed for $TiSiO_4$. Therefore, further research is needed in order to characterize the structural, vibrational, and electronic properties of $TiSiO_4$ at ambient and high-pressure. Density-functional theory (DFT) calculations have proved to be an efficient tool to improve the understanding of the main physical properties of many oxides related to $TiSiO_4$.[16,24,25] In this work, DFT will be employed to study $TiSiO_4$.

The aim of our research is to investigate the physical properties of $TiSiO_4$ at ambient and high pressure. We used the CRYSTAL06 code[26] to perform DFT calculations of the crystal total-energy as a function of the volume. We also carried out lattice-dynamic and band-structure calculations. The refractive index of $TiSiO_4$ was characterized too. We found that at ambient pressure $TiSiO_4$ crystallizes in the $CrVO_4$-type structure, being an indirect band-gap semiconductor with a band-gap energy (E_g) of 3.49 eV. Upon compression, two phase transitions are predicted to take place to the zircon-type and scheelite-type structures at 0.8 and 3.8 GPa, respectively. The low-pressure phase is more compressible than other silicates having a bulk-modulus (B_0) of 124 GPa, but the high-pressure phases show considerable smaller compressibilities than $ZrSiO_4$. Section II gives the computational details of the reported calculations. In Sec. III we describe the three crystal structures taken into account in this work. In Sec. IV the obtained results are presented and discussed. Finally, our conclusions are collected in Sec. V.

II. METHODOLOGY

Calculations were performed with the CRYSTAL06 program package.[26] For the titanium atom, the 6-31G basis set devel-

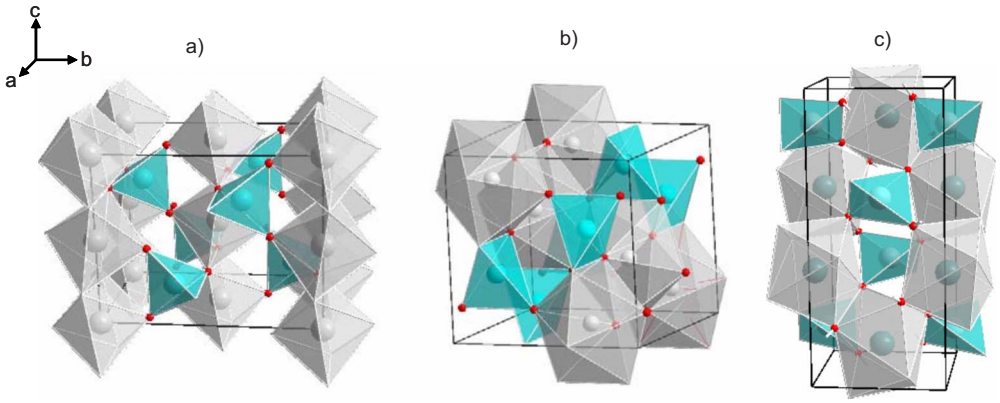

FIG. 1. (Color online). Structures of $TiSiO_4$ a) $CrVO_4$-type, (b) zircon and (c) scheelite. SiO_4, TiO_6, and TiO_8 polyhedra are shown.

oped by Rassolov *et al.*[27] was modified by omitting the function of the lowest exponent of the three describing the valence *sp* orbitals, and setting 1.0 as the *s* and *p* coefficients and $\alpha=0.0840$ for the exponent of the outermost *sp* shell, as in previous papers.[28–30] Oxygen and silicon atoms have been described by the standard 6-31G* and 6-21G** basis set, respectively. The optimized exponent of the *d* shell for O was $\alpha=0.8$ and those for the most external *sp* and *d* shells for Si were, $\alpha=0.3$ and $\alpha=0.5$, respectively. The Becke's three-parameter hybrid nonlocal exchange functional[31] combined with the Lee-Yang-Parr gradient-corrected correlation functional, B3LYP,[32] has been used. Hybrid density-functional methods have been extensively used for molecules, providing an accurate description of crystalline structures, bond lengths, binding energies, and band-gap values.[33] The diagonalization of the Fock matrix was performed at adequate *k*-points grids (Pack-Monkhorst 1976) in the reciprocal space, 21, 13, and 14 *k* points for orthorhombic, zircon and scheelite phases, respectively. The thresholds controlling the accuracy of the calculation of Coulomb and exchange integrals were set to 10^{-8} (ITOL1 to ITOL4) and 10^{-14} (ITOL5), whereas the percent of Fock/Kohn-Sham matrices mixing was set to 40 (IPMIX=40).[26] A total optimization procedure (FULLOPT) of the studied structures was made taking into account as starting point the cell parameters and internal positions of isomorphic $CrVO_4$,[23] $ZrSiO_4$ (zircon),[34] $CaWO_4$ (scheelite),[34] and other structures commonly found in ABO_4 oxides. To compute the pressure effect, we find the values of the geometrical parameters that minimize *E* at a number of fixed volumes using the external Melder-Mead algorithm,[35] assuring a convergence in total energy better than 10^{-6} a.u. in all cases. A fitting procedure of the computed energy-volume data with the Birch-Murnaghan[36] equation of state provides values of zero-pressure bulk modulus and its pressure derivative as well as enthalpy-pressure curves for the three studied polymorphs.[37]

Band structures have been obtained along the appropriate high-symmetry paths of the Brillouin zone. Vibrational frequencies calculation in CRYSTAL was performed at the Γ point.[26] The dynamical matrix was computed by numerical evaluation of the first-derivative of the analytical atomic gradients. The point group symmetry of the system was fully exploited to reduce the number of points to be considered. On each numerical step, the residual symmetry was preserved during the SCF process and the gradients calculation. Vibrational frequencies were computed at the Γ point within the harmonic approximation. Finally, to calculate the high-frequency dielectric constant with CRYSTAL, in a first step the response of the system to a static, constant electric field is calculated by adding to the Hamiltonian operator a periodic electric field. The number of unit cells in the applied field direction was 4, and 40 points were chosen for the Fourier transformation. By collecting a set of dielectric tensor values as a function of the external electric field applied, we can then evaluate the high-frequency dielectric constant (ε_∞) with a fitting procedure.

III. SELECTED STRUCTURES

One of the characteristics of pressure-induced phase transitions in ABO_4 compounds is the tendency to increase the coordination number for both A and B cations.[21] In particular, a systematic explanation of the crystal structures of many ABO_4 oxides at ambient and high pressure has been proposed based upon the cation A and cation B radii.[21] This systematic predicted precisely the high-pressure structural sequence recently reported for ABO_4 vanadates.[38] In the case of $TiSiO_4$, it suggests three candidate structures for this compound, $CrVO_4$-type, zircon-type, and scheelite-type. These and other structures frequently found in ABO_4 compounds [monoclinic $CoMoO_4$-type (SG: $C2/m$, $Z=8$), wolframite (SG: $P2/c$, $Z=2$), and M-fergusonite (SG: I2/a, $Z=4$) and orthorhombic barite-type (SG: *Pnma*, $Z=4$) have been considered in our calculations. As we will discus latter, $CrVO_4$-type, zircon-type, and scheelite-type are the energetically most competitive structures in the pressure range covered by our work. Since these are crystalline structures to which the reader may not be familiarized with, we provide in the following a brief description of them.

A. Orthorhombic $CrVO_4$-type polymorph

Figure 1(a) shows a detail of the orthorhombic $CrVO_4$-type structure proposed for $TiSiO_4$, which belongs to space group *Cmcm*. The framework structure of this polymorph is comprised of nearly regular edge-sharing octahedra of TiO_6. In addition, the silicon atoms occupy the tetrahedral interstitial sites constructed by cubic close-packed oxygen

atom arrays. In the figure, it can be seen that the TiO_6 octahedra form chains that propagate in the *c* axis, with these chains linked one to another by SiO_4 tetrahedra. These tetrahedra share corners with the TiO_6 octahedral units of the chains. The main difference between this structure and the tetragonal structures is the lower coordination of the Ti cation (coordination number six instead of eight). $CrVO_4$ type is also the less densely packed structure among those here considered.

B. Tetragonal zircon-type polymorph

Figure 1(b) shows a detail of the tetragonal zircon-type structure proposed for $TiSiO_4$, which belongs to space group $I4_1/amd$. This structure consists of isolated SiO_4 tetrahedra, elongated parallel to the *c* axis, sharing corners and edges with TiO_8 triangular dodecahedra, which can be described as two interpenetrating TiO_4 tetrahedra. These dodecahedra share edges which each other to form chains parallel to the *c* axis [see Fig. 1(b)]. The chains are joined laterally by four edge-sharing dodecahedra, two in each of the crystallographically equivalent directions, *a* axis and *b* axis. The chains of TiO_8 polyhedra are crossed linked by sharing corners with SiO_4 tetrahedra. The SiO_4 and TiO_8 polyhedra also form an edge-connected chain of alternated SiO_4 and TiO_8 polyhedra parallel to the *c* axis, between which lie unoccupied channels. These edge-connected chains comprise an especially strong feature in the structure as manifested in many physical properties of zircon-type oxides.[39]

C. Tetragonal scheelite polymorph

Figure 1(c) shows a detail of the tetragonal scheelite-type structure proposed for $TiSiO_4$. Many ABO_4 compounds, with A and B atoms having valence +4, crystallize in this structure (space group: $I4_1/a$). From the cationic point of view, the scheelite structure consists of two intercalated diamond lattices: one for A cations and another for B cations. In the scheelite-type polymorph of $TiSiO_4$, the titanium cations are coordinated by eight oxygen anions with two different distances, thus forming TiO_8 polyhedral units. On the other hand, silicon cations are coordinated by four O anions, forming relatively isolated SiO_4 tetrahedral units. The TiO_8 dodecahedra in scheelite share edges with adjacent TiO_8 polyhedra, forming zigzag chains along the *c* axis. These chains are crossed linked through SiO_4 tetrahedra by sharing corners with them [see Fig. 1(c)]. Scheelite and zircon are structures related via crystallographic twin operations.[40] Among their similarities it should be noted that both structures show identical coordination environment. However the SiO_4 tetrahedra in zircon are less distorted than those in the scheelite structure, moreover, the latter structure is more densely packed than the former.

IV. RESULTS AND DISCUSSION

A. Structural stability, EOS fittings, and local compressibility

Figure 2 shows the energy-volume curve for the different polymorphs of $TiSiO_4$. From it, the relative stability and coexistence pressures of the phases can be extracted by the common-tangent construction. For $TiSiO_4$ we found that at ambient conditions the most stable phase is the $CrVO_4$-type one. This structure has been previously observed in vanadates, phosphates, chromates, sulphates, and selenates,[23] but never before in a silicate. In addition, two phase transitions are predicted to take place subsequently to the zircon and scheelite phases at 0.8 and 3.8 GPa. The structural parameters of each phase are summarized in Table I. The atomic positions obtained for the different structures are similar to those of isomorphic ABO_4 compounds; e.g., $CrVO_4$,[23] ZrSiO4 (zircon),[41] and $CaWO_4$ (scheelite).[42] Also the anisotropy of scheelite and the orthorhombic structure are similar to that of compounds of their family. In contrast, for the zircon phase we obtained a large value for the c/a axial ratio (0.944) in comparison with the rest of the zircons in which usually $c/a<0.91$. A similar exception to this characteristic has been observed in $ThGeO_4$ ($c/a=0.936$), being attributed to a strong repulsion between the Th and Ge cations.[43] This fact suggests that the repulsion between Ti and Si in zircon-type $TiSiO_4$ is larger than that between Zr (Hf) and Si in zircon (hafnon).

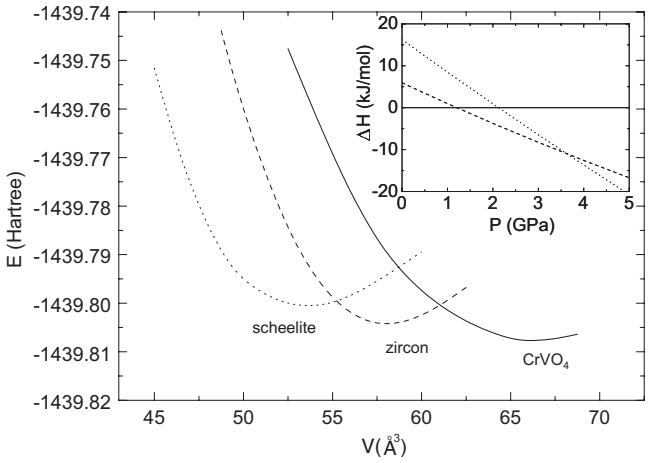

FIG. 2. Internal energy (Hartree) *versus* volume ($Å^3$) per formula unit. The entalphy versus pressure curve for the $TiSiO_4$ polymorphs is depicted in the inset (taking the $CrVO_4$-type structure as reference). In the figure we only show the results for those structures which are relevant for $P<25$ GPa.

The fact that the $CrVO_4$-type phase is the most stable structure at ambient conditions is in good agreement with the predictions made from the systematic drawn for ABO_4 compounds using the Bastide's diagram.[21] This analysis predicts that increasing the A cationic radius tends to increase the coordination of this ion. In our case, Ti has a smaller ionic radius (0.605 Å for coordination 6) than Zr and Hf (0.84 and 0.83 Å), and therefore a smaller coordination for the Ti cation is expected in $TiSiO_4$ than for Zr and Hf in $ZrSiO_4$ and $HfSiO_4$. This is exactly what is found when the $CrVO_4$-type structure (Ti six-coordinated) is compared with the zircon-type structure (Ti eight-coordinated). Indeed, $TiSiO_4$ falls into the stability field expected for the $CrVO_4$-type structure in the structural-field map reported by Errandonea and Manjon.[21] The finding that $TiSiO_4$ has a $CrVO_4$-type structure is also consistent with the fact that $TiPO_4$ and $TiVO_4$ crystallize in the $CrVO_4$-type structure[40] while $ScPO_4$ and

TABLE I. Structural parameters and bulk properties for the $TiSiO_4$ polymorphs.

	$CrVO_4$			Zircon				Scheelite		
a (Å)	5.2957			6.2570 (6.21)[a]				4.5536		
b (Å)	7.9996			6.2570 (6.21)[a]				4.5536		
c (Å)	6.2554			5.9351 (5.81)[a]				10.1277		
V (Å^3)	66.3			58.1 (56.0)[a]				52.5		
Ti (x,y,z)	0	0	0	0	0.75	0.125	0	0.25	0.625	
Si (x,y,z)	0	0.3470	0.25	0	0.25	0.375	0	0.25	0.125	
O_1 (x,y,z)	0	0.2284	0.0414	0	0.0578 (0.0591)[a]	0.1918 (0.0591)[a]	0.2651	0.0719	0.0471	
O_2 (x,y,z)	0.2527	0.4707	0.25							
B (GPa)	124.0	136.6		248.4	274.4		238.2	267.1		
B'	4.7	4		5.3	4		6.6	4		
$d_{Ti\text{-}O}$ (Å)	1.842	2.052		1.966 (1.95)[a]	2.232(2.19)[a]		1.979	2.200		
$d_{Si\text{-}O}$ (Å)	1.611	1.664		1.621			1.655			

[a]Data from Reference 19.

$ScVO_4$ crystallize in the zircon-type structure (ionic radius for Sc=0.87 Å).[44]

In the inset of Figure 2 we illustrate the enthalpy-pressure curve computed for $TiSiO_4$ (taking the $CrVO_4$-type structure as reference). At the transition pressure, P_t, the relative volume change is calculated as $\Delta V_t=[V_2(P_t)\text{-}V_1(P_t)]/V_1(P_t)$ where 2 and 1 stand, respectively, for the final and initial phases involved. At 0.8 GPa our results show a transition from $CrVO_4$ type to the zircon phase, with a large-volume change of 11.8%. At 3.8 GPa a transition from zircon to scheelite is obtained with a significant volume reduction of 8.5%. As we mentioned above, other structures have been also considered in other calculations. However, we found they are not stable from ambient pressure to 25 GPa. Some of them, like the M-fergusonite structure are good candidates to be a postscheelite structure at $P>25$ GPa, but this possible transition is beyond the scope of this work. We also considered a possible decomposition of $TiSiO_4$ into its simple oxides (SiO_2+TiO_2) taking into account the different polymorphs observed for TiO_2 and SiO_2 below 25 GPa. We found that decomposition is energetically not competitive with the three polymorphs of $TiSiO_4$ that are predicted to stabilize below 25 GPa. From our calculations we also obtained the equation of state (EOS) for the three phases of $TiSiO_4$. The obtained EOS parameters are shown in Table I.

An analysis of these results points out that the $CrVO_4$-type structure has a computed zero-pressure bulk modulus of 124 GPa. However, a higher value of 137 GPa is obtained when the compression data are fitted by fixing the bulk-modulus pressure derivative $B_0'=4$. The computed bulk modulus of zircon is 248 and 274 GPa (with $B_0'=4$). This value is in good agreement with the 265 GPa value predicted from an empirical model that consider that in zircon-type and scheelite-type structures B_0 is related to the cation charge density of the TiO_8 polyhedra.[21] For scheelite, we obtain 238 and 267 GPa (with $B_0'=4$), which is similar to the $B_0=270$ GPa value obtained according to phenomenological model.[21] These results suggest that the low-pressure phase of $TiSiO_4$ is more compressible than any of the tetragonal phases. This observation is consistent with the fact that the $CrVO_4$ type is an open structure fill with voids in-between the different polyhedra (see Fig. 1). This fact allows that a volume reduction of the structure could be induced not only by a Si-O and Ti-O bond length reduction, but also by a tilting of the SiO_4 tetrahedra, allowing a larger bulk compressibility than in zircon and scheelite. The large compressibility of $CrVO_4$-type $TiSiO_4$ is also consistent with the high-pressure behavior observed in orthophosphates. Indeed, $CrVO_4$-type $AlPO_4$ has a B_0 of 127 GPa (similar to $CrVO_4$-type $TiSiO_4$),[45] while zircon-structured phosphates such as $YbPO_4$ and $LuPO_4$ present a B_0 close to 200 GPa.[46] Note that also $CrVO_4$-type oxides have usually a much larger thermal expansivity than zircon-type and scheelite-type oxides,[47] which also supports the different mechanical properties we found for the orthorhombic structure.

It is interesting to comment here, that according to these results, tetragonal $TiSiO_4$ can be considered an ultralow compressibility silicate in spite that the Si atom is not highly coordinated on it (Si-O coordination 4). The high incompressibility of the zircon and scheelite phases indicates that probably octahedrally coordinated silicon is not necessarily required to generate ultrastiff silicates. Apparently, $TiSiO_4$ zircon and scheelite are the most incompressible materials containing SiO_4 tetrahedra. Based upon correlations between incompressibility and hardness, scheelite-structured $TiSiO_4$ may thus represent a potential ultrahard material. Indeed, stishovite SiO_2 (Si six-coordinated) has a B_0 of 292(13) GPa,[48] i.e., comparable to that of the HP phases of $TiSiO_4$. Note that the zircon-scheelite transition is usually a first-order nonreversible transition. This suggest than uncompressible scheelite-type TiSiO4 could be possible quenched from high-pressure to ambient pressure, favoring its production using large-volume presses.[49]

Changes in observable properties induced by the phase transitions can be also related to different local atomic ar-

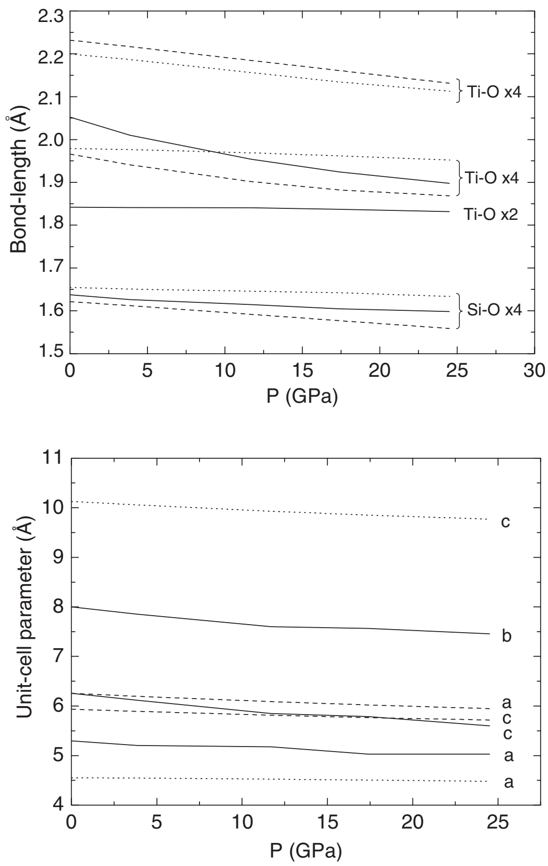

FIG. 3. Evolution with pressure of (a) bond distance and (b) unit-cell parameters. Solid, dashed and dotted lines represents $CrVO_4$-type, zircon, and scheelite phases, respectively.

rangements in the crystals. Thus the higher density of the tetragonal structures can be traced back to the unit-cell volume reduction due to a more effective packing of the O atoms surrounding the Ti atoms. In this way, the atomic displacements across the $CrVO_4$ type to the zircon transition are clearly related to the environment evolution of the Ti cation. For example, around P_t, the orthorhombic phase has 2+4 Ti-O distances of 1.842/2.052 Å, respectively, and four Si-O distances of 1.638 Å. The distortion of the TiO_6 octahedra is reduced by pressure since the large equatorial distances are most compressible than the short axial distance (see Fig. 3). On the other hand, at the same pressure, the 4+4 Ti-O and the four Si-O shortest distances in the zircon phase are 1.966/2.232 Å and 1.621 Å, respectively. Therefore, in the first pressure-induced transition, we find that the silicon coordination does not change and the Si-O bond lengths remain almost unmodified, whereas the titanium coordination increases and the Ti-O bond lengths become larger, to make the formation of new bonds feasible. Thus, the relatively short Ti-O bonds in the orthorhombic phase become larger in the eightfold coordination of the tetragonal phases but the higher coordination enhances their strength and brings their compressibility close to that shown by the Si-O bonds. As a consequence of this, the high-pressure phases have the ultralow compressibility described above.

Figure 3 shows the evolution of both Si-O and Ti-O bond distance with pressure. A comparison of the bond lengths of the zircon and scheelite polymorphs suggests that the Si–O bonds of the SiO_4 tetrahedra are relatively a little longer for scheelite compared to the same bond in the zircon phase. On the other hand, they are 10% more compressible in zircon than in scheelite. Besides, in the case of the TiO_8 polyhedron, four of eight Ti-O bonds are 25% more compressible in zircon than in scheelite having the other four distances similar compressibility. These observations are in good agreement with the fact that the scheelite structure is more densely packed than the zircon one.

To close this section we would like to mention that the compression of the $CrVO_4$-type structure is more anisotropic than that of the zircon and scheelite phases. This can be seen in Fig. 3(b), where the variation of unit-cell parameters with pressure is shown. In particular, the c axis of the orthorhombic structure is the most compressible one. For it, we obtained the following linear compressibilities κ_c (0.0042 GPa^{-1}) $> \kappa_b$, (0.0027 GPa^{-1}) $\cong \kappa_a$, (0.0021 GPa^{-1}). The large compressibility of the c axis is due to the fact that the TiO_6 octahedra chains are aligned along this axis whereas along the other directions SiO_4 and TiO_6 units are intercalated. Therefore, since pressure produces basically a reduction of the Ti-O bonds, the c axis should be the most compressible axes in the $CrVO_4$-type phase. Compression in zircon and scheelite is also nonisotropic, but the differences between linear compressibilities are not as large as in the orthorhombic phase. For zircon and scheelite $TiSiO_4$ we found the following values of κ_c (0.0020 and 0.0012 GPa^{-1}, respectively) which are slightly higher than κ_a, (0.0014 and 0.0007 GPa^{-1}, respectively). Therefore, in both structures c/a decreases upon compression. This behavior is typical of scheelite-structured oxides,[50,51] but the opposite is usually observed in zircon-type oxides.[36] We think this behavior could be related with the exceptionally large c/a ratio of zircon $TiSiO_4$. Probably compression compensates the Ti-Si repulsion making this structure more similar to that of other zircon-structured oxides.

B. Phonon frequencies at the Γ point

Group theoretical considerations lead to the following vibrational representation at the Γ point for scheelite in the standard notation:

$$\Gamma_{\text{scheelite}} = (3A_g + 3B_u) + (5B_g + 5A_u) + (5E_g + 5E_u),$$

A and B modes are nondegenerate, whereas the E modes are doubly degenerate. Among these modes, one A_u and one E_u correspond to the acoustic modes, being the rest optic modes. In scheelites, the first member of the pairs is Raman active and the second member is infrared (IR) active, except for the B_u silent modes that are not IR active. Consequently, we expect 13 zone-center Raman-active modes in scheelite,

$$\Gamma_{\text{scheelite}} = 3A_g + 5B_g + 5E_g.$$

Group theory predicts the following vibrational representation for zircon:

TABLE II. Phonon frequencies and Grüneisen parameters for $CrVO_4$-type, zircon and scheelite phases (Raman modes).

$CrVO_4$			Zircon				Scheelite		
Mode	$\omega(0)$ cm^{-1}	γ	Mode	$\omega(0)$ cm^{-1}	ω^a cm^{-1}	γ	Mode	$\omega(0)$ cm^{-1}	γ
$T(A_g)$	215.17	1.45	$T(E_g)$	211.61	194.3	−1.77	$T(B_g)$	235.95	−0.11
$T(B_{1g})$	270.51	0.46	$T(B_{1g})$	248.69	258.9	3.55	$T(E_g)$	256.60	1.36
$R(B_{1g})$	328.34	2.27	$T(E_g)$	254.34	242.4	1.12	$T(B_g)$	292.66	0.35
$R(B_{2g})$	337.99	0.02	$T(B_{1g})$	300.16	262.9	−1.96	$T(E_g)$	375.11	0.59
$T(B_{3g})$	379.86	1.93	$\nu_2(A_{1g})$	416.45	383.2	1.88	$R(A_g)$	400.42	1.68
$R(B_{3g})$	466.62	1.24	$R(E_g)$	428.61	430.1	2.71	$\nu_2(A_g)$	412.71	0.84
$\nu_2(A_g)$	474.80	0.98	$\nu_2(B_{2g})$	433.89	417.6	1.69	$\nu_2(B_g)$	511.83	0.51
$\nu_4(B_{1g})$	538.18	0.50	$\nu_4(E_g)$	592.72	544.3	0.92	$R(E_g)$	531.92	0.70
$\nu_2(B_{2g})$	538.60	1.18	$\nu_4(B_{1g})$	674.85	627.2	1.26	$\nu_4(E_g)$	594.63	0.80
$\nu_4(A_g)$	583.54	0.59	$\nu_1(A_{1g})$	966.07	1011.4	2.01	$\nu_4(B_g)$	698.67	0.58
$\nu_4(B_{3g})$	692.00	0.64	$\nu_3(E_g)$	976.56	945.4	2.01	$\nu_3(B_g)$	889.55	0.81
$\nu_3(B_{1g})$	837.95	0.76	$\nu_3(B_{1g})$	1077.50	1047.2	2.10	$\nu_1(A_g)$	930.96	0.66
$\nu_3(A_g)$	962.28	0.45					$\nu_3(E_g)$	974.19	0.79
$\nu_1(A_g)$	1014.14	0.57							
$\nu_3(B_{3g})$	1070.41	0.51							

[a]Raman modes data from Reference 19.

$$\Gamma_{\text{zircon}} = (2A_{1g} + B_{1u}) + (B_{2g} + A_{1u}) + (A_{2g} + 2B_{2u}) + (4B_{1g} + 4A_{2u}) + (5E_g + 5E_u).$$

Among these 26 modes 12 are Raman active $\Gamma_{\text{zircon}}=2A_{1g}+4B_{1g}+B_{2g}+5E_g$ and 7 are IR active $(3A_{2u}+4E_u)$. The rest of the modes are acoustic $(A_{2u}+E_u)$ or silent modes $(B_{1u}+A_{2g}+A_{1u}+2B_{2u})$.

Group theory predicts that the $CrVO_4$-type structure supports 36 modes which decompose as follows:

$$\Gamma_{\text{Cmcm}} = (5A_g + 6B_{1u}) + (4B_{1g} + 3A_u) + (2B_{2g} + 7B_{2u}) + (4B_{3g} + 5B_{3u}),$$

15 modes are Raman active $\Gamma_{\text{Cmcm}}=5A_g+4B_{1g}+2B_{2g}+4B_{3g}$ and other 15 are active in the IR $(5B_{1u}+6B_{2u}+4B_{3u})$. The rest of the modes are acoustic $(B_{1u}+B_{2u}+B_{3u})$ or silent $(3A_u)$ modes.

The Raman spectra of the structures of interest can be interpreted in terms of modes of the SiO_4 tetrahedra, which can be considered as independent units in the structures. Thus, the scheelite, zircon, and $CrVO_4$ modes can be classified either as internal (the SiO_4 center of mass does not move) or as external (movements of the SiO_4 tetrahedra as rigid units). The assignment of the different vibrational modes according with this description can be seen in Tables I–III.

The internal modes of the SiO_4 units are usually named as: ν_1 (symmetric stretching), ν_2 (symmetric bending), ν_3 (asymmetric stretching), and ν_4 (asymmetric bending). Modes related to pure rotation or translation of the SiO_4 units are denoted as R and T, respectively. The translational modes are usually the lowest in frequency, the internal modes are the highest in frequency, and the frequencies of the rotational modes are between those of the translational and the internal modes.

In Table II we give the mode assignment of the different Raman-active phonon frequencies of the three structures together with the Grüneisen parameters, $\gamma=[B_0/\omega(0)]d\omega/dP$, which have been calculated with the B_0 values reported in Table I. We also provide the same information for infrared modes in Table III. The phonon frequencies calculated for the zircon structure agree reasonable well with those reported by Rignanese *et al.*[19] The only mode for which a considerable frequency difference is obtained is the rotational Raman-active $R(E_g)$ mode for which we found a frequency of 428 cm^{-1} and previously a frequency of 544 cm^{-1} was reported.

The analysis of the Raman-active modes of the three polymorphs shows that the tetragonal phases present soft modes, i.e. $T(E_g)$ at 212 cm^{-1} and $T(B_{1g})$ at 300 cm^{-1} for the zircon and the $T(B_g)$ at 236 cm^{-1} for the scheelite phase. These modes are characterized by a decrease of the vibrational frequency with pressure (negative Grüneisen parameter). This feature is typical of scheelite-structure oxides[52] and suggests that at higher pressure scheelite-type $TiSiO_4$ should undergo a transition involving a strong coupling between a zone-centre optic mode and a strain of B_g symmetry. In addition to the softening of low-frequency zircon and scheelite Raman modes, we obtain the same behavior for some silent modes, inactive for both IR and Raman experiments. For the zircon polymorph, two of these $[R(B_{1u})$ and $R(A_{2g})]$ are very soft, and correspond to vibration modes of zircon in which the SiO_4 tetrahedra rotate as a unit.

In Tables II and III, it can be seen that for the three studied structures there is a phonon gap between the frequencies of the internal stretching modes and the rest of the modes. This is typical of ABO_4 oxides and is basically related to the fact that the ν_1 and ν_3 modes involve movements of the less

TABLE III. IR modes.

$CrVO_4$			Zircon				Scheelite		
Mode	$\omega(0)$ cm^{-1}	γ	Mode	$\omega(0)$ cm^{-1}	ω^a cm^{-1}	γ	Mode	$\omega(0)$ cm^{-1}	γ
$T(B_{1u})$	147.18	2.53	$T(E_u)$	307.96	303.4	−0.09	$T(A_u)$	274.76	−0.09
$T(B_{1u})$	239.64	0.60	$T(A_{2u})$	335.05	318.7	2.69	$T(E_u)$	296.20	2.69
$T(B_{2u})$	259.49	0.61	$R(E_u)$	410.68	374.1	0.44	$\nu_4(A_u)$	363.36	0.44
$T(B_{2u})$	391.54	0.23	$\nu_4(E_u)$	447.26	433.1	2.70	$R(E_u)$	413.20	2.70
$T(B_{3u})$	412.89	0.10	$\nu_4(A_{2u})$	638.03	606.4	1.30	$\nu_4(E_u)$	546.95	1.30
$R(B_{1u})$	423.91	1.56	$\nu_3(E_u)$	906.49	876.7	2.17	$\nu_2(A_u)$	649.56	2.17
$R(B_{3u})$	444.87	0.41	$\nu_3(A_{2u})$	1032.56	1000.3	2.17	$\nu_3(A_u)$	841.21	2.17
$\nu_2(B_{2u})$	510.74	1.34					$\nu_3(E_u)$	888.57	
$\nu_4(B_{3u})$	524.75	0.81							
$\nu_3(B_{3u})$	613.26	1.07							
$\nu_4(B_{1u})$	665.62	0.27							
$\nu_4(B_{2u})$	809.25	0.73							
$\nu_1(B_{2u})$	888.20	0.84							
$\nu_3(B_{1u})$	943.74	0.80							
$\nu_3(B_{2u})$	994.40	0.32							

[a]Transverse optic infrared modes data from Reference 19.

compressible bonds of the crystal (Si-O). In addition, these modes can be well correlated with the stretching vibrations of the free-ion $(SiO_4)^{-4}$ molecule and those of SiO_4 tetrahedra in SiO_2 polymorphs.[53] This fact supports the assumption that the frequency modes of $TiSiO_4$, as a first approximation, can be separated between internal and external vibrations. It is interesting to compare the frequencies of zircon $TiSiO_4$ with other zircon-type silicates. All of them show similar spectra with a 300 cm^{-1} phonon gap between the internal stretching modes and the rest of the modes. Usually, also the frequency of the highest frequency mode can be correlated mass of the transition metal cation. Indeed the $\nu_3(B_{1g})$ mode has a frequency of 1009 cm^{-1} in $ZrSiO_4$ and of 1018 cm^{-1} in $HfSiO_4$; i.e., the heaviest the metal cation the largest the phonon frequency.[54] Therefore, a frequency smaller than 1009 cm^{-1} is expected for the same mode in $TiSiO_4$, which suggests that the calculated frequencies can slightly overestimate the phonon frequencies of $TiSiO_4$.

To close this section, it is interesting to note that the IR phonons predicted for the orthorhombic phase of $TiSiO_4$ (the one stable at ambient conditions) are very similar in frequency with the IR vibrations measured in amorphous films of $TiSiO_4$. In particular, the amorphous Ti-O-Si and Si-O-Si stretching vibrations[20,55] found around 930 and 1000 cm^{-1}, respectively, the Si-O-Si bending vibration observed near 800 cm^{-1}, and the Ti-O vibration located about 430 cm^{-1}, coincide with the IR modes predicted for $CrVO_4$-type $TiSiO_4$. We think this is not a mere coincidence, and can be due to the fact that the local order of amorphous $TiSiO_4$ is similar to that of crystalline $TiSiO_4$. The growth of amorphous $TiSiO_4$ with pulsed-laser deposition and chemical-vapor deposition can be due to the presence of a kinetic barrier that precludes the formation of crystalline $TiSiO_4$ at the growing conditions. Probably, the combination of high-pressure and high-temperature conditions could lead to a successful preparation of crystalline $TiSiO_4$.

C. Electronic structure

The calculated band structures of $TiSiO_4$ were constructed along the appropriate high-symmetry directions of the corresponding irreducible Brillouin zones using the calculated lattice parameters listed in Table I. $TiSiO_4$ at ambient pressure is a direct band-gap material, with the gap at the Γ point of the Brillouin zone (BZ) and E_g=3.49 eV. Thus, it offers a larger band gap and band offset with Si than rutile TiO_2 [E_g=3.0 eV (Ref. 56)], which constitute and advantage for the reduction of the tunneling leakage current in MOSFET devices.

For zircon-type $TiSiO_4$ the band gap is located at the Γ-point of the Brillouin Zone corresponding to a direct transition, whereas the scheelite and the orthorhombic $CrVO_4$-type phases present an indirect transition from Γ to Σ (in the path $\Gamma \rightarrow Z$) and from Γ to S points of the corresponding BZ, respectively. Note that the direct band gap at Γ for the scheelite structure is 4.30 eV very close to the minimum indirect band gap. To the best of our knowledge there are no experimental works exploring the electronic structure of the $TiSiO_4$ system. However, the band-gap reported for scheelite $TiSiO_4$ is similar to that of most of scheelite ABO_4 compounds,[57] which gives support to our predictions. The analysis of the band structure reveals that in all the studied phases the highest occupied band and the one immediately beneath are of $2p$ (O) character and depend on the Ti-O bond. The overlap between $2p$ (O) and $3d$ (Ti) crystal orbitals is stronger than that between $2p$ (O) and 3p (Si) ones.

The conduction bands (CB) arise from $4s$ and $3d$ states of Ti atoms with their bottom located at the Γ point for the zircon polymorph. The bottom of the CB in the scheelite phase is situated at Σ in the path between Γ and Z points, near Z, the first band of the CB is very flat, the gap is indirect but the direct gap at Γ presents a very close value. These features resemble the band structure reported for other ABO_4

TABLE IV. Values of dielectric constant, ε_∞, refractive index, n, and band-gap energy, E_g, at ambient pressure.

Phase	α-SiO_2	TiO_2		Zircon		Scheelite		$CrVO_4$-type		
Component	isotropic	∥	⊥	∥	⊥	∥	⊥	[100]	[010]	[001]
ε_∞(this work)										
ε_∞[a]	1.93	7.21 6.66[a]	5.92 8.81[a]	4.41 5.52[a]	4.48 5.56[a]	4.67	4.83	2.99	4.07	3.71
n (this work)										
n[a]	1.39	2.68 2.58[a]	2.43 2.97[a]	2.10 2.35[a]	2.12 2.36[a]	2.16	2.20	1.73	2.02	1.93
n (exp)	1.48[b]	[2.87[c]–2.58[d]][e]								
	1.46[d]	[2.74[d]–2.48[d]][f]								
	1.45[3]	2.55[3]								
E_g (this work)				4.50		4.27			3.49	

[a]Calculated from Reference 19.
[b]α-SiO_2 (633 nm) (Reference 67).
[c]Extraordinary.
[d]Ordinary.
[e]Fused quartz and rutile (633 nm) (Reference 68).
[f]Rutile (1064 nm) (Reference 68).

scheelites.[58] In the case of the orthorhombic $CrVO_4$-type phase the electronic structure is characterized by an indirect band gap since the top of the bottom of the CB is located at the S (0,1/2,0) reciprocal space point. Here the direct energy gap at Γ is 3.52 eV very close also to the indirect value (E_g=3.49 eV).

The effect of the pressure on the band structures of all polymorphs is also examined in the present study. The zero-pressure values of the band-gap energy (E_g) are as follow: $CrVO_4$-type (3.49 eV), zircon (4.50 eV), and scheelite-type (4.27 eV). The variation of the band gap with pressure, dE_g/dP, for the zircon structure is positive with a value of 25.8 meV GPa^{-1}. The electronic structure of the scheelite phase is less deformable and also positive, being the corresponding value of dE_g/dP 7.3 meV GPa^{-1}. On the other hand, the orthorhombic (*Cmcm*) phase presents a negative value of −25.4 meV GPa^{-1} for dE_g/dP. DFT calculations can slightly overestimate the absolute value of E_g, however, they are known to be very precise in the determination of dE_g/dP.[59] Therefore, our predictions for dE_g/dP would be helpful to understand the pressure behavior of the band structure of orthosilicates. Unfortunately, at the moment no previous estimations for these parameters in orthosilicates are available to compare with. However, from our calculations we can predict a large band-gap opening at the $CrVO_4$-zircon transition (ΔE_g=1 eV) and a small band-gap collapse at the zircon-scheelite transition (ΔE_g=0.3 eV). In addition, the possible blue shift of the band gap of scheelite $TiSiO_4$ with pressure is consistent with the behavior of other covalent compounds such as spinel-structured oxides.[60]

D. Dielectric permitivity

The response of crystals to external electric fields determines their dielectric behavior. To compute the dielectric constant the main difficulty is the nonperiodic nature of the macroscopic electric potential, meaning that the methods based on Bloch's theorem do not apply. The trick chosen herein to overcome this problem is the use of a "sawtooth" potential in conjunction with a supercell scheme for maintaining the periodicity along the applied field direction, as proposed by Kunc and Resta.[61] In the present work, the finite field sawtooth scheme implemented in the CRYSTAL06 code is used.[62] This method, although more expensive in terms of computational power and time than for example the variational approach proposed by Souza *et al.*,[63] has been used successfully for calculating the dielectric constants and the nonlinear indices of periodic systems.[64–66]

By collecting a set of dielectric tensor values as a function of the external applied electric field we can then evaluate the electronic permittivity tensor or high-frequency dielectric constant (ε_∞) as well as the refractive index, $n=\sqrt{\varepsilon_\infty}$. The calculated values of ε_∞ and n at ambient pressure are reported in Table IV. The tetragonal phases present two independent components of ε_∞, $\varepsilon_\parallel$ and $\varepsilon_\perp$, parallel and perpendicular to the c axis, respectively. The $CrVO_4$-type phase presents three independent components parallel to each axis. For comparison purposes, we also report the calculated values of ε_∞ and n for SiO_2 (α-cristobalite) and TiO_2 (rutile) together with previous experimental and theoretical data. As expected, $TiSiO_4$ has a dielectric constant in-between those of TiO_2 and SiO_2. In addition, its value increases as the packing efficiency increases in the high-pressure phases. Regarding the zircon-type phase, the parameters calculated for us are around 20% smaller than those calculated by Rignanese.[19] Similar differences are found for TiO_2, but our results agree better with the experimental results (see Table IV). However, both works agree in suggesting that $TiSiO_4$ is a potential high-κ dielectric. Finally, we would like to stress that apparently the anisotropy of the dielectric properties is more notorious for the low-pressure orthorhombic structure of $TiSiO_4$ than for the zircon and scheelite structures.

V. SUMMARY

We have studied the mechanical, dynamical, and electronic properties of $TiSiO_4$ at ambient and high pressure by

means of DFT, lattice-dynamic and band-structure calculations. We found that at ambient conditions $TiSiO_4$ is predicted to crystallize in an orthorhombic structure isomorphic to $CrVO_4$. This is the first time that such structure is reported for a silicate. Upon compression, two phase transitions are predicted to take place to the tetragonal zircon-type and scheelite-type structures at 0.8 and 3.8 GPa, respectively. The scheelite phase remains stable at least up to 25 GPa. Note that based upon crystallochemical arguments[21,40] a similar structural sequence is also possible for different oxides isomorphic to $CrVO_4$ (vanadates, phosphates, chromates, sulphates, and selenates). We also determined the EOS for the three phases of $TiSiO_4$, finding that the low-pressure phase is more compressible than other silicates having a bulk-modulus B_0 of 124 GPa. However, the high-pressure phases show extremely low compressibilities. Phonon frequencies for the different structures are also reported, being the different modes assigned based upon our calculations and assuming that in the different structures the SiO_4 tetrahedra are nearly isolated units. The pressure evolution of different phonons is also described. Finally, the dielectric constants, refractive index and band structure of the different phases of $TiSiO_4$ are reported. According to our calculations, $TiSiO_4$ is a wide band-gap semiconductor, with a high dielectric constant, which upon compression could become an ultrahard material. All these features make of $TiSiO_4$ an interesting candidate for many technological applications.

ACKNOWLEDGMENTS

Financial support from Spanish MALTA-Consolider Ingenio 2010 Program (Project No. CSD2007-00045) is gratefully acknowledged. This work was partially supported by the Spanish MICCIN under Grant No. MAT2007-65990-C03-01.

[1] X. Gao and I. E. Wachs, Catal. Today **51**, 233 (1999).
[2] X. Wang, H. Masumoto, Y. Someno, and T. Hirai, Thin Solid Films **338**, 105 (1999).
[3] S. M. Lee, J. H. Park, K. S. Hong, W. J. Cho, and D. L. Kim, J. Vac. Sci. Technol. A **18**, 2384 (2000) and reference therein.
[4] M. F. Ouellette, R. V. Lang, K. L. Yan, R. W. Bertram, and R. S. Owles, J. Vac. Sci. Technol. A **9**, 1188 (1991).
[5] Y. Sorek, R. Reisfeld, I. Filkenstein, and S. Rushkin, Appl. Phys. Lett. **63**, 3256 (1993).
[6] X. Orignac, D. Barbier, X. M. Du, and R. M. Almeida, Appl. Phys. Lett. **84**, 2304 (2004).
[7] D. K. Sarkar, E. Desbiens, and M. A. El Khakani, Appl. Phys. Lett. **80**, 294 (2002).
[8] D. Brassard, D. K. Sarkar, L. Ouellet, and M. A. El Khakani, J. Vac. Sci. Technol. A **22**, 851 (2004).
[9] A. Nishiyama, A. Kaneko, M. Koyama, Y. Kamata, I. Fujiwara, M. Koike, M. Yoshiki, and M. Koike, Mater. Res. Soc. Symp. Proc. **670**, K4.8.1 (2001).
[10] T. Kamada, M. Kitagawa, M. Shibuya, and T. Hirao, Jpn. J. Appl. Phys., Part 1 **30**, 3594 (1991).
[11] R. M. Hazen and L. W. Finger, Am. Mineral. **64**, 196 (1979).
[12] *Reviews in Mineralogy and Geochemistry*, edited by J. M. Hanchar and P. W. O. Hoskin (Mineralogical Society of America, Washington, DC, 2003), Vol. 53.
[13] R. C. Ewing, Proc. Natl. Acad. Sci. U.S.A. **96**, 3432 (1999).
[14] S. Rios and T. B. Ballaran, J. Appl. Crystallogr. **36**, 1006 (2003).
[15] K. Trachenko, V. V. Brazhkin, O. B. Tsiok, M. T. Dove, and E. K. H. Salje, Phys. Rev. Lett. **98**, 135502 (2007).
[16] M. Marqués, M. Florez, J. M. Recio, L. Gerward, and J. Staun Olsen, Phys. Rev. B **74**, 014104 (2006).
[17] E. Knittle and Q. Williams, Am. Mineral. **78**, 245 (1993).
[18] B. Manoun, R. T. Downs, and S. K. Saxena, Am. Mineral. **91**, 1888 (2006).
[19] G. M. Rignanese, X. Rocquefelte, X. Gonze, and A. Pasquarello, Int. J. Quantum Chem. **101**, 793 (2005).
[20] D. Brassard and M. A. El Khakani, J. Appl. Phys. **98**, 054912 (2005).
[21] D. Errandonea and F. J. Manjón, Prog. Mater. Sci. **53**, 711 (2008).
[22] D. Errandonea, M. Somayazulu, and D. Häusermann, Phys. Status Solidi B **235**, 162 (2003).
[23] B. C. Frazer and P. J. Brown, Phys. Rev. **125**, 1283 (1962).
[24] R. Lacomba-Perales, D. Errandonea, D. Martinez-Garcia, P. Rodríguez-Hernández, S. Radescu, A. Mujica, A. Muñoz, J. C. Chervin, and A. Polian, Phys. Rev. B **79**, 094105 (2009).
[25] L. Gracia, A. Beltrán, J. Andrés, R. Franco, and J. M. Recio, Phys. Rev. B **66**, 224114 (2002).
[26] R. Dovesi, V. R. Saunders, C. Roetti, R. Orlando, C. M. Zicovich-Wilson, F. Pascale, B. Civalleri, K. Doll, N. M. Harrison, I. J. Bush, Ph. D'Arco, and M. Llunell, *CRYSTAL06 User's Manual* (University of Torino, Torino, 2006).
[27] V. A. Rassolov, J. A. Pople, M. A. Ratner, and T. L. Windus, J. Chem. Phys. **109**, 1223 (1998).
[28] A. Beltrán, L. Gracia, and J. Andrés, J. Phys. Chem. B **110**, 23417 (2006).
[29] M. Calatayud, P. Mori-Sanchez, A. Beltrán, A. M. Pendás, E. Francisco, J. Andrés, and J. M. Recio, Phys. Rev. B **64**, 184113 (2001).
[30] A. Beltrán, J. Andrés, J. R. Sambranso, and E. Longo, J. Phys. Chem. A **112**, 8943 (2008).
[31] A. Becke, J. Chem. Phys. **98**, 5648 (1993).
[32] C. Lee, W. Yang, and R. G. Parr, Phys. Rev. B **37**, 785 (1988).
[33] C. H. Hu and D. P. Chong, *Encyclopedia of Computational Chemistry* (Wiley, Chichester, 1998).
[34] J. A. Melder and R. Mead, Comput. J. **7**, 308 (1965).
[35] F. Birch, J. Geophys. Res. **57**, 227 (1952).
[36] M. A. Blanco, E. Francisco, and V. Luaña, Comput. Phys. Commun. **158**, 57 (2004).
[37] D. Errandonea, R. Lacomba-Perales, J. Ruiz-Fuertes, A. Segura, S. N. Achary, and A. K. Tyagi, Phys. Rev. B **79**, 184104 (2009).
[38] W. van Westrenen, M. R. Frank, Y. Fei, J. M. Hanchar, R. J. Finch, and Ch. Sh. Zha, J. Am. Ceram. Soc. **88**, 1345 (2005) and reference therein.
[39] H. Nyman, B. G. Hyde, and S. Andersson, Acta Crystallogr. B

40, 441 (1984).
[40] E. Baran, J. Mater. Sci. **33**, 2479 (1998).
[41] W. Binks, Mineral. Mag. **21**, 176 (1926).
[42] R. M. Hazen, L. W. Finger, and J. W. E. Mariathasan, J. Phys. Chem. Solids **46**, 253 (1985).
[43] A. Ennaciri, A. Kahn, and D. Michel, J. Less Common Met. **124**, 105 (1986).
[44] A. T. Aldred, Acta Crystallogr. B **40**, 569 (1984).
[45] S. M. Sharma, N. Garg, and S. K. Sikka, Phys. Rev. B **62**, 8824 (2000).
[46] F. X. Zhang, M. Lang, R. C. Ewing, J. Lian, Z. W. Wang, J. Hu, and L. A. Boatner, J. Solid State Chem. **181**, 2633 (2008).
[47] R. J. Riedner and L. Cartz, J. Appl. Phys. **42**, 5177 (1971); C. V. Reddy, K. S. Muthy, and D. Kistaieb, J. Phys. C **21**, 863 (1988).
[48] T. Yamanaka, J. Synchrotron Radiat. **12**, 566 (2005).
[49] D. Errandonea, Y. Meng, D. Hausermann, and T. Uchida, J. Phys.: Condens. Matter **15**, 1277 (2003).
[50] D. Errandonea, Phys. Status Solidi B **242**, R125 (2005).
[51] D. Errandonea, R. S. Kumar, X. Ma, and C. Y. Tu, J. Solid State Chem. **181**, 355 (2008).
[52] D. Errandonea and F. J. Manjon, Mater. Res. Bull. **44**, 807 (2009).
[53] P. Gillet, A. Le Cheach, and M. Modan, J. Geophys. Res. **95**, 21635 (1990).
[54] R. W. G. Syme, D. J. Lockwood, and H. J. Kerr, J. Phys. C **10**, 1335 (1977).
[55] Z. M. Yang, Q. Fang, J. Y. Yang, J. X. Wu, Y. Di, W. Chen, M. L. Chen, and I. W. Boyd, Thin Solid Films **453-454**, 167 (2004).
[56] J. Pascual, J. Camassel, and H. Mathieu, Phys. Rev. B **18**, 5606 (1978).
[57] R. Lacomba-Perales, J. Ruiz-Fuertes, D. Errandonea, D. Martínez-García, and A. Segura, EPL **83**, 37002 (2008).
[58] Y. Zhang, N. A. W. Holzwarth, and R. T. Williams, Phys. Rev. B **57**, 12738 (1998).
[59] N. E. Christensen, Phys. Rev. B **30**, 5753 (1984).
[60] J. Ruiz-Fuertes, D. Errandonea, F. J. Manjón, D. Martínez-García, A. Segura, V. V. Ursaki, and I. M. Tiginyanu, J. Appl. Phys. **103**, 063710 (2008).
[61] K. Kunc and R. Resta, Phys. Rev. Lett. **51**, 686 (1983).
[62] M. Rérat, C. Darrigan, G. Mallia, M. Ferrero, and R. Dovesi, Crystal Tutorial Project, http://www.crystal.unito.it
[63] I. Souza, J. Íñiguez, and D. Vanderbilt, Phys. Rev. Lett. **89**, 117602 (2002).
[64] G. Mallia, R. Dovesi, and F. Corà, Phys. Status Solidi B **243**, 2935 (2006).
[65] C. Darrigan, M. Rérat, G. Mallia, and R. Dovesi, J. Comput. Chem. **24**, 1305 (2003).
[66] M. Ben Yahia, E. Orhan, A. Beltrán, O. Masson, T. MerleMéjean, A. Mirgorodski, and P. Thomas, J. Phys. Chem. B **112**, 10777 (2008).
[67] J. M. Weber, *Handbook of Optical Materials* (CRC Press, Boca Raton, FL, 2003).
[68] M. R. Shenoy and R. M. De La Rue, IEE Proc.-J: Optoelectron. **139**, 163 (1992).